Technique to obtain positron emission mammography images in registration with x-ray mammograms

Alanah M. Bergman,[a),b)] Christopher J. Thompson, Kavita Murthy, James L. Robar,[b)] Raymond L. Clancy, and Michael J. English
Montreal Neurological Institute, 3801 University Street, Montreal Québec H3A-2B4, Canada

Antoine Loutfi, Robert Lisbona, and Jean Gagnon
Royal Victoria Hospital, 687 Pine Avenue, Montreal Québec H3A 1A1, Canada

(Received 18 June 1997; accepted for publication 2 September 1998)

X-ray mammograms reveal abnormal tissue densities, while metabolic images identify regions of abnormal metabolism. Conventional nuclear medicine and radiologic breast images must be acquired at different times with different patient positions making coregistration difficult. Accurate coregistration of metabolic and x-ray images of the breast is likely to be important when acquiring information about the location and diagnosis of suspicious lesions or tumors. Our PEM-1 (positron emission mammography) system detects metabolic activity within the breast. The two planar detectors are integrated into a conventional x-ray mammography unit. This arrangement simplifies the image registration process by allowing a breast metabolic image to be acquired immediately after performing an x-ray mammogram. The patient is not moved between procedures. A coregistration tool has also been developed. A thin plastic sheet with a wire frame protrudes from the side of the upper PEM detector. With the tool positioned over the suspicious area of the breast, a magnified film density image is made using the available x-ray equipment. A radio-opaque rectangular outline of the wire frame is visible on the film image. During a positron emission metabolic scan, detectors acquire a 49×59 mm^2 image of the same region. The PEM detectors can be positioned anywhere along the width of the breast. This provides an image of a particular region of interest. Several contiguous images may be combined to provide a complete scan. © *1998 American Association of Physicists in Medicine.* [S0094-2405(98)01311-X]

Key words: breast cancer, FDG, coregistration, PEM

I. INTRODUCTION

X-ray mammography is currently the imaging technique of choice for detection of breast cancer. However, this technique has limited sensitivity and specificity. Dense tissue masses found within the breast are regarded as suspicious lesions. Using mammography it is difficult to differentiate dense but healthy breast tissue from a dense tumor. Many (65%–85%)[1] breast biopsies based on suspicious mammography findings return a negative diagnosis for breast cancer after pathological examination of the excised tissue. Alternatively, a tumor may have a similar density to healthy tissue, so some (5%–15%) of cancers are not detected with mammography.[2]

In 1930 Warburg *et al.*[3] first described enhanced glucose metabolism in tumors compared with healthy normal tissues. Recently Brown *et al.*[4] showed that the increased glucose uptake in breast tumors is facilitated by an increased expression of the glucose transporter molecule GLUT-1 (in response to hypoxic conditions within the tumor). 2-[F-18]-flouro-2-deoxy-D-glucose (FDG) is a positron emitting glucose analog that is widely used for metabolic imaging with positron emission tomography (PET). FDG and glucose enter cells via the same membrane transport mechanisms. The metabolites of FDG accumulate preferentially in tumor cells. Normal cells also accumulate FDG, but at a reduced rate compared to the active tumor cells. This provides the contrast needed to identify tumors against a background of normal tissue. The accumulation of FDG in different tissues can be measured quantitatively using PET. A FDG PET study by Wahl *et al.*[5] in breast cancer patients demonstrated a mean tumor to background ratio of 8.1:1 (range 1.8–$>$800, 25 tumors, size ''3.0 cm''–''8×12 cm''). Tse *et al.*[6] reported that 12/14 breast cancer patients showed positive FDG uptake. Nieweg *et al.*[7,8] reported 11/12 cases of primary breast cancer were detected with FDG-PET, with only one lesion, which was under 1 cm, being missed. A study of 97 breast tumor patients with FDG studies by Avril *et al.*[9] is the most extensive series published so far. They found a sensitivity of 90% and a specificity of 85% when applying full quantification to their images. Avril states that motion artifacts and small lesions caused a loss of sensitivity in their results.

We have applied the basic principles of (PET) technology to a dedicated breast imaging instrument.[10–12] Our positron emission mammography (PEM-1) instrument has been developed to image tumors within the moderately compressed breast by taking advantage of the increased FDG uptake. The term ''positron emission mammography'' refers to any instrument, regardless of its geometry or image reconstruction algorithm, which is designed to detect the presence of positron emitting isotopes within breast tissues. Recently other PEM instrument designs have been reported.[13–17] The first

clinical PEM study was reported by Weinberg *et al.*[13] in 1996.

PEM can determine if a suspicious lesion has an abnormal metabolic rate, implying the presence of cancerous cells. This suggests that it will have an important role as a secondary cancer screening technique (after mammography, but before biopsy). We anticipate that PEM will eventually be able to detect these changes in metabolism quantitatively. This would provide a useful tool for assessing a tumor's response to anticancer drugs and radiation therapy.[18,19] Tumors, which respond to a variety of treatments, generally have much a lower FDG uptake than they did before the onset of therapy.[20,21] A recent study by Bassa *et al.*,[22] has shown a significant decrease in tumor glucose metabolism in response to an effective course of chemotherapy.

Comparing images obtained from different modalities has traditionally been an obstacle. For example, conventional nuclear medicine and radiologic breast images must be acquired at different times with different patient positions. In practice, methods employed for image registration include the use of positioning devices to align the patient, external and internal landmarks, and relatively complex mathematical algorithms.[23,24] Accurate coregistration of metabolic and x-ray mammography images of the breast provides a valuable approach to identifying, localizing, and quantifying changes in breast anatomy and glucose metabolism. Combining x-ray mammography and metabolic imaging into one unit simplifies the registration process by allowing for consecutive images to be acquired without moving the patient between scans.

II. EQUIPMENT

A. PEM detectors

Construction details of the PEM scanner have been described in a previous paper by Thompson *et al.*[10] Briefly, the detectors are comprised of two $72\times72\times20\ \mathrm{mm}^3$ pixellated bismuth germinate scintillation crystal block arrays. The two planar detectors are positioned 180° relative to each other and they operate in coincidence to detect the 511 keV annihilation photons from positron decay. The crystals are cut from both sides of the block (11.5 mm depth on one side and 6.5 mm depth on the other) with the separation between cuts being 2.0 mm. The cuts are offset 1 mm on both sides giving a sampling distance of 1.0 mm. The crystals are optically coupled to Hamamatsu R3941-05 position-sensitive photomultiplier tubes (PS-PMT).

The signals from each PS-PMT are processed to produce X, Y position and energy information about each photon interaction. Timing signals from the last dynode of each detector are processed by a constant fraction discriminator and a coincidence circuit. Valid coincidences are used to trigger an Aurora-14 6-channel CAMAC analog to digital converter (ADC) which digitizes the energy and position signals. The ADC is interfaced to a DEC Alpha workstation. The workstation is on a cart with the data acquisition system mounted below. In practice, it stands in one corner of the mammography examination room. The PEM and x-ray images are available during the patient examination. This greatly facilitates acquisition of additional PEM images and retakes of the mammograms, if necessary, to optimize lesion visibility.

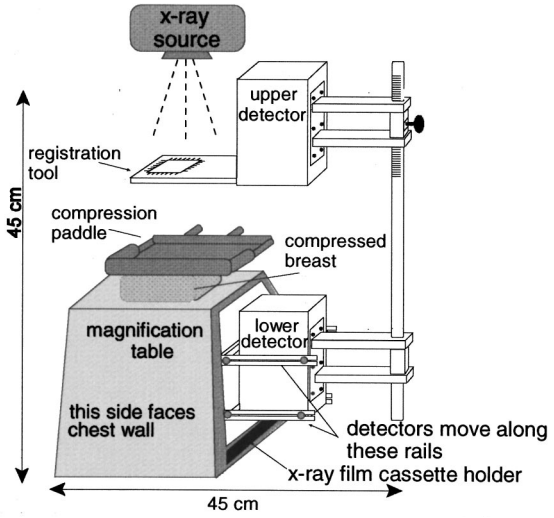

FIG. 1. The integration of PEM detectors (white areas) into a conventional mammography unit (shaded areas). The PEM detectors are shown retracted to allow an x-ray mammogram to be performed. The PEM detectors slide to the left of the figure to perform the PEM scan.

B. X-ray mammography films

The x-ray mammography film images are acquired on a Philips Mammo DIAGNOST-UC unit. Standard diagnostic mammography film is used. The developed films are placed on a light box and digitized using a Panasonic WV-BL-200 video camera connected to the Alpha workstation. The raw video image has 512×480 pixels. The pixels in the raw video image are interpolated in order to make them square. The resulting matrix size is 512×380 pixels. The size of the pixels depends on the setting on the video camera's zoom lens.

C. Integration of PEM and x-ray mammography

The PEM detectors have been integrated into a conventional Philips mammography unit as illustrated in Fig. 1. Each detector is housed in a shielded aluminum box. A standard mammography magnification table has been modified such that the PEM system will attach securely onto the structure of the x-ray unit. The magnification table is a hollow box conventionally used to establish a fixed amount of distance between the breast and the x-ray film cassette.

The two PEM detectors are mounted on rails in order to scan the entire breast width. The detectors always move in tandem. During an x-ray mammogram, the detectors slide out of the x-ray photon field allowing an unobstructed film image to be acquired. The maximum height of the magnification table/PEM detector assembly is 45 cm. The width of the instrument varies from 30 to 46 cm depending on the lateral position of the detectors. A plastic compression

paddle is used to immobilize the breast. The compression paddle attenuates approximately 2%–3% of the 511 keV gamma rays.

The biggest problem with this design has been the positioning of the detectors over suspicious regions that are within 2.5 cm of the chest wall. Here we have found that mediolateral oblique views allow for deeper imaging.

III. PEM IMAGE ACQUISITION

A. PEM software

The PEM software consists of three interdependent programs to acquire, compute, or accept commands, and display the images. The command program is used to select various options: identify the patient; digitize a mammogram; redisplay previous images, etc. It also performs the backprojection and corrections described below. During the examination, the display program provides an almost ''real-time'' display of seven transverse PEM images corresponding to seven slice depths through the compressed breast. (The images are normally updated every 5 s.) The display program is an x-windows application. The display allows the user to control the image contrast, color table, and to load a selected image into one of three auxiliary windows for further processing. These windows allow one selected image to be filtered, to produce profiles used to measure the lesion contrast and size, and to register the PEM image with the mammogram.

B. Image formation

The X and Y positioning information for each detector is used to identify discrete crystal elements at both ends of a line of response through the breast volume.[10] Extensive use is made of look-up tables, which are loaded as required.[12] Limited angle backprojection is used to form PEM images which are oriented transverse to the patient's body.[10] With this method, a number of image planes can be viewed. We have chosen to display seven planes through the thickness of the compressed breast (Fig. 2). To form the images a number is added to the pixel in each plane through which the line joining the two coincident crystals passes. This number in inversely proportional to the product of the crystals' relative detection efficiencies, the attenuation of the gamma rays along their oblique path through the breast, and the detection probability had the annihilation occurred at that location in the plane, as shown in our previous work.[10] The image plane closest to the site of high focal uptake has the best focused image of the site. The seven PEM images are presented left to right with the left-most image nearest the x-ray source. The image orientation is as if the breast were pendant with the chest wall at the top of the image. The pixel size in the seven 128×128 images is 0.5 mm since the sampling distance on each detector is 1.0 mm.

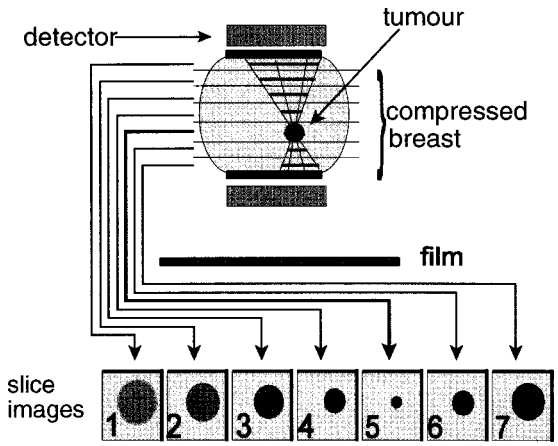

FIG. 2. Formation of seven images by backprojection of lines of response through a compressed breast. The images are displayed in the primary window from left to right with the leftmost image nearest the x-ray source. The best focused hot-spot image (thick line) corresponds to the plane of the region of higher uptake.

IV. COREGISTRATION OF IMAGES

A. Coregistration tool

In order to facilitate the registration between the radiographic and the metabolic images, a coregistration tool has been developed. The registration tool is a thin sheet of Plexiglas™ ($130\times95\times3$ mm thick) with a 39×49 mm^2 window and graticule made of 0.5-mm-thick steel wire. The coregistration tool can be seen extending from the upper detector in Fig. 1. These wires are visible on the x-ray image and provide magnification information. In Fig. 3 the window dimensions are given as $\mathbf{L}_X$ and $\mathbf{L}_Y$. The nearest edge of the window to the patient is located $\mathbf{W}_{YO}$ from the edge of the film.

The PEM field of view[10] (49×59 mm^2) is larger than the coregistration tool window. Since the tool window is positioned above the breast, its image is always magnified more than any plane through the breast, on the x-ray film. Depending of the compression used, the window size will reach at least the 49×59 mm^2 at the midpoint of the breast.

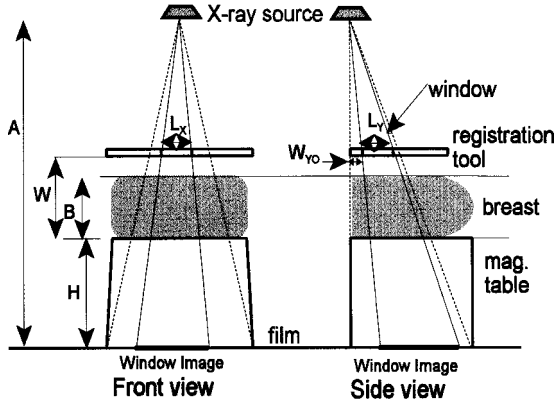

FIG. 3. Magnification of PEM images in frontal and lateral views showing how the window in the registration is imaged on the mammogram film.

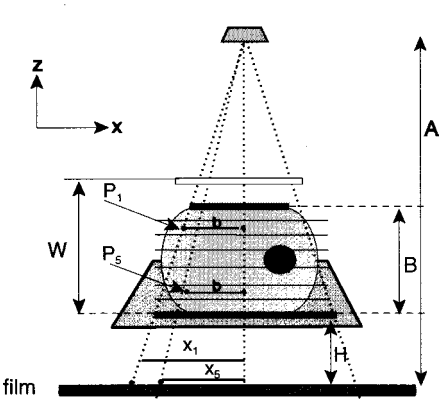

FIG. 4. Front view of PEM magnification geometry showing two points in different PEM slices, both the same distance from the center line. Since they are on different slices their images will appear at different points in the mammogram.

During the x-ray examination, the breast is imaged through this window, producing a radio-opaque grid on the film. The window provides a landmark which can be used to position the PEM data on top of the x-ray mammography image. This region can be repositioned by sliding the tool/detector assembly across the breast area.

B. Derivation of magnification factors

During a mammogram, x rays diverge from a point on the anode producing a magnified film image of the patient's breast. The mammography film is not symmetric since the anode of the x-ray source is directly above the *center of the chest wall edge* of the mammography film. This point is the origin of the magnification on the x-ray film as shown in Fig. 3. Figure 3 shows both frontal and lateral views. The seven PEM image planes are each magnified by a different amount, and appear shifted by a different amount on the mammogram.

The PEM image must be scaled by a factor which depends on the PEM image plane chosen (one of **seven**) and the zoom setting on the video camera. This is illustrated in Fig. 4 where two points labeled $\mathbf{P}_1$, in plane **1**, and $\mathbf{P}_5$ in plane **5** are both a distance **b** from the center of the **X**-axis PEM image. If these points were radio-opaque each would cast a different shadow on the film, one at $\mathbf{X}_1$, and the other at $\mathbf{X}_5$.

The program calculates the necessary scale factors required to match the PEM image size to the film image size by considering the similar triangles constructed when photons are emitted from the point like x-ray anode (see Fig. 4). Suppose the x-ray anode is at a height **A**, and the window in the tool is at a height **W** above the magnification table. If the height of the magnification table is **H**, and the thickness of the compressed breast is **B** then from similar triangles, the magnification $\mathbf{M}_{Ss}$ of the X coordinate of a point $\mathbf{P}_S$ in slice number ''S'' is

$$M_S=\frac{A}{A-H-B(7.5-S)/7}. \tag{1}$$

TABLE I. Symbols, definitions, and values for distances which influence the PEM magnification values.

Distance	Symbol	Value (mm)
Anode to film	A	580
Height of magnification table	H	220
X length of window	L_X	39
Y length of window	L_Y	49
Y origin of window from film edge	W_{YO}	26
Distance from window to breast	W_B	36
Breast compression (variable)	B	15-70
Distance from window to magnification table (variable)	W	51-106
Horizontal distance from window to PEM	D_{WP}	150

Similarly, the magnification of the window, $\mathbf{M}_W$, is

$$M_W=\frac{A}{A-H-W}. \tag{2}$$

Combining Eqs. (1) and (2) we obtain an expression for the relative magnification of the PEM slice S with respect to the image of the window, $\mathbf{M}_{SW}$:

$$M_{SW}=\frac{M_S}{M_W}=\frac{A-H-W}{A-H-B[(7.5-S)/7]}. \tag{3}$$

The edge of the window nearest the patient's chest is located $\mathbf{W}_{YO}$ mm from a vertical line joining the anode to the back of the film as shown in Fig. 3. The location of this line on the film is $M_W * W_{YO}$ from the edge. This distance is a reference to the edge of the film when it is digitized. The window is always a fixed distance, $\mathbf{W}_B$, above the compressed breast (36 mm). Table I lists these symbols and gives the values (in mm) for our instrument.

The PEM detectors traverse along the width of the breast. To correlate the image of the registration tool on the x-ray film with the field of view of the PEM scanner, the detectors must move across the breast by a specific distance. A scale on the railings is provided for this purpose. The distance that the detectors would have to move to align the two modalities is not simply equal to the physical distance, D_{WP}, between the plastic coregistration window and the PEM detector (150 mm). This effect is illustrated in Fig. 5. In practice, since the error is relatively small, the detectors are always moved by a fixed distance (corresponding to a breast thickness of 50 mm, and the lesion being in the central slice) and a software correction is applied. The PEM image is moved by a small amount, Δx depending on the actual slice of the lesion and breast compression. From similar triangles:

$$\frac{X_M}{A-H-0.5B}=\frac{d}{A-H-W},$$

$$\Delta x=X_M-X_P, \tag{4}$$

$$\Delta x=d\left[\frac{A-H-0.5B}{A-H-W}\right]-X_P,$$

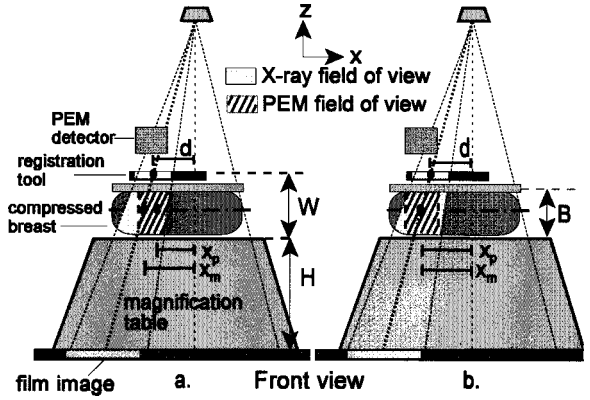

FIG. 5. (a) Center of field of view of mammogram (X_m) and PEM image (X_p) do not match if one assumes that the position of the PEM scanner should correspond exactly to the previous position of the registration tool. (b) Applying the magnification corrections ensures that the same region is imaged.

where $\mathbf{X}_P$ is the center of the PEM image field, and $\mathbf{X}_M$ is the center of the registration window in the mammogram, and **0.5B** is the height of the center slice through the breast.

C. PEM/mammogram coregistration software

We have written software to display PEM images using standard X-Windows library functions in Open VMS. Users have several options when presented with the seven PEM image planes on the computer screen. After selecting one of the images, zoom, smoothing, and profile features allow for further image processing.

The PEM image overlays the x-ray image in a ''registration window.'' The PEM and x-ray images have separate color scales whose upper and lower thresholds can be chosen by the user. When overlaying the PEM image on the mammogram, the PEM color is displayed if the pixel is above the lower PEM display threshold, otherwise the grayscale mammogram pixel is displayed. The resulting effect is a background grayscale mammogram image with colored regions highlighting areas of increased FDG radio-tracer uptake.

In order for the PEM images to be displayed with the same scale as the mammogram it is necessary to account for the zoom factor of the video camera used to digitize the film. This, and the user identification of the coregistration tool described below, require an additional scale factor between mammogram pixels and PEM pixels. Due to the fact that the video camera pixels may not be perfectly square, and the user may not identify the corners of the registration tool perfectly, separate scale factors for each axis $\mathbf{S}_X$ and $\mathbf{S}_Y$ are used. These are incorporated into Eq. (3) to provide a pair ($\mathbf{M}_{SWX}$ and $\mathbf{M}_{SWY}$) of factors to scale the PEM pixels to digitized mammogram pixels:

$$M_{SWX}=S_X\frac{A-H-W}{A-H-B[7.5-S/7]},$$
$$M_{SWY}=S_Y\frac{A-H-W}{A-H-B[7.5-S/7]}. \quad (5)$$

The scaled PEM image is offset by Δx before being overlaid on the mammogram.

The procedure used to display the PEM image on the mammogram consists of four phases, the first two of which require user input. *First:* The user selects a grayscale range which maximizes the visibility of the coregistration tool on the digitized mammogram. *Second:* The user selects the ''Find Tool'' option, and uses the mouse to drag and stretch a rectangular outline of the registration tool until it overlays the tool's image on the digitized x-ray film. (During this phase the scale factors, $\mathbf{S}_X$ and $\mathbf{S}_Y$, for each axis of the mammogram image are established. This allows for any zoom setting to be used on the digitizing camera.) *Third:* The program interpolates PEM image to the size of the mammogram, and its position is established. *Fourth:* The program displays the PEM pixels in the offset and aligned PEM image which exceed the lower PEM color-scale threshold on the mammogram image. The result is a metabolic breast image scaled and aligned with the anatomical features visible on the mammogram.

V. PHANTOM EXPERIMENTS

A. Magnification factors

To verify the magnification factors, the tool was placed at three heights, 120, 60, and 5 mm above the magnification table, exposing the film at each height. The film was then digitized and the tool was aligned with each image on the film. The measured coregistration tool and image slice magnification factors were compared with calculated values.

B. Image of diamond pattern of capillary tubes

A diamond-shaped array of 22, 0.5-mm-i.d. capillary tubes was filled with ^{18}F solution to a depth of 1 cm (using the capillary action of the tube). The closest tube center to center distance was 5.7 mm. This arrangement was imaged in air to facilitate the precise correlation between a PEM image and its corresponding mammogram. The glass tubes are easily seen on the x-ray mammography film. An x-ray mammogram and a PEM image were made for several different lateral positions along the detectors' range of motion. Seven lateral displacements, from -30 to $+30$ mm, from the x-ray axis of symmetry were used. Seven sets of images were collected for two equivalent breast compressions (60 and 70 mm).

The image registration procedure is used to align each image pair. A feature of the registration software allows the user to identify and store the coordinates of different points in an image. (This feature was written for making initial offset calibrations for the PEM/x-ray mammogram system but is it not required clinically.) The image threshold is first set to optimize the presentation of the PEM image. The centers of the tubes which are in the field of view of the PEM detectors are then identified. After thresholding the combined image so that the PEM image disappears, but the x-ray mammogram remains, the center of each tube on the film image is identified. The paired differences in both X and Y

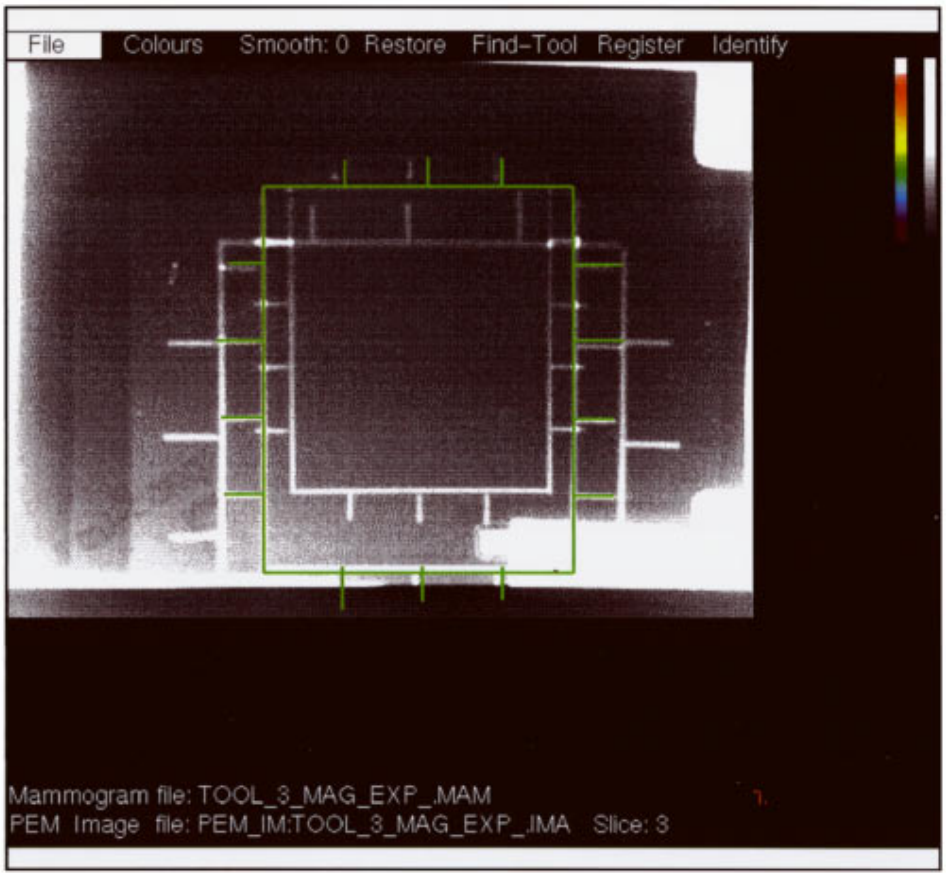

FIG. 6. The coregistration tool corresponding to breast compressions of 5, 60, and 120 mm. The green pattern corresponds to the digital representation of the tool which has been scaled to indicate the image of the tool at 60 mm compression.

coordinates measured for each modality are then used to estimate the mean distance between the PEM and x-ray images. (The sign is positive if the point in the PEM image is to the right of, or above the same point in the mammogram.) The standard deviation of the differences between the center of each point in the PEM image and each point in the x-ray image for each image set was also calculated. A nonzero mean distance can be due to the difficulty in reading the scale at both ends of the detector travel, and any play in the vertical and horizontal rails along which the detectors slide. A nonzero standard deviation would be due to the image resolution and the ability of the user to identify the center of each point in each image.

TABLE II. Magnification factors calculated for the coregistration tool from Eq. (2), and measured for two slices and breast compressions equivalent to 5, 60 and 120 mm. (The measured values include zoom factors and errors in scaling the tool.)

Equivalent breast compression (mm)	Calculated coregistration tool magnification	Measured slice magnification (X,Y)	
		Slice 1	Slice 7
5	1.82	1.28, 1.23	1.26, 1.22
60	2.20	1.48, 1.42	1.27, 1.22
120	2.84	1.76, 1.73	1.26, 1.25

VI. PATIENT STUDIES

The initial clinical trial using this instrument is presently underway. The trial requires examination of 20 patients with symptoms very suspicious of breast cancer. So far 13 subjects have been studied. A detailed analysis of the outcome of these studies will be presented elsewhere.

This scanning protocol forms part of the grant application to the National Cancer Institute of Canada's Canadian Breast Cancer Research Initiative, under which this research is being carried out. The protocol has been approved by the Royal Victoria Hospital's Research Ethics Board. The patients must be older than 21 years of age, nondiabetic, not pregnant, and be a candidate for an excisional breast biopsy or mastectomy within two weeks. Preference is given to patients with small lesions (less than 1 cm in diameter). They must give informed consent in French or English using an approved form.

Patients fast for at least 4 h, and are injected with 75 MBq of ^{18}F FDG in the Nuclear Medicine department of the Royal Victoria Hospital. This injected dose is approximately 1/5 of the amount used for conventional whole-body PET studies. This lower dose can still be imaged effectively because of the high sensitivity of the PEM instrument compared to PET.

They are then taken to the Cedars Breast Clinic where they are encouraged to drink water. Before preparation for

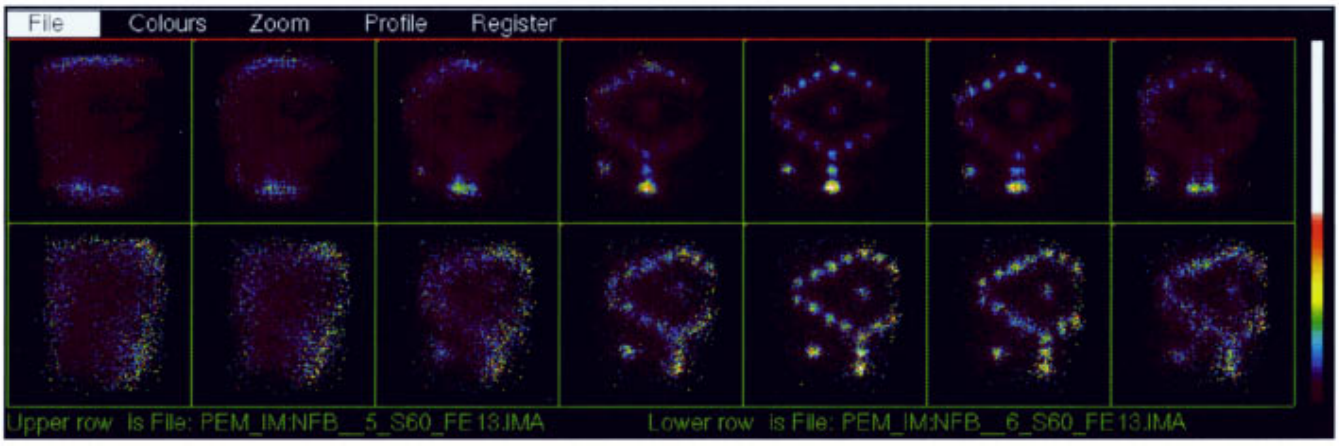

FIG. 7. Pattern of ^{18}F filled capillary tubes imaged in the center of the PEM field of view (top row), and displayed by 10 mm (bottom row) to demonstrate the field of view. The top row images have 60 000 counts and the bottom row images have 14 000 counts.

the PEM scan, they are asked to urinate in order to reduce their radiation exposure. Based on previous mammograms, the suspicious breast is placed on the magnification table, and semicompressed. The compression used is less than that required for a diagnostic mammogram due to the length of the subsequent PEM scan (1–5 min). Either a cranial-caudal (CC) or medio-lateral oblique (MLO) mammogram is performed through the registration window attached to the upper PEM detector. Due to the reduced breast compression, the resultant film image may not be of diagnostic or screening quality, however, the suspicious mass should still be clearly visible. After viewing the film, the PEM detectors are positioned over the same suspicious area and a 1–5 min metabolic scan is performed. A scan of the ''assumed normal'' breast is also performed.

To obtain optimal image quality, our protocol allows other views to be acquired, if necessary, given that the patient is willing to tolerate further examination. Additional x-ray studies are only made if a change in orientation (from CC to MLO, for example) is required. If the PEM detectors are only moved laterally to enhance the image, the new position is recorded, but an additional mammogram film is not made. A PEM scan of the contralateral breast is also made in order to obtain images from ''probably normal'' breasts without requiring the scanning of assumed ''normal subjects.''

VII. RESULTS

A. Magnification factors

Figure 6 shows the result of a triple exposure mammogram film of the coregistration tool at heights equivalent to breast compressions of 5, 60, and 120 mm. The green outline is the digital model of the tool which has been overlaid on the 60 mm exposure. The tool outline was also overlaid on the two other images.

The magnification factors calculated for the registration tool in all three cases are given in Table II, along with the measured magnification factors for the extreme slices through the breast (slices 1 and 7) as estimated by the program using Eq. (1). Table II shows the range of magnification factors for extreme (5 and 120 mm) and typical (60 mm) values of breast compression. It also demonstrates that the magnification of the upper slices through the breast changes much more than the lowest slice as a function of breast compression.

B. Diamond pattern phantom

Figure 7 shows the seven images of the array of glass capillary tubes filled with ^{18}F solution. The detector separation was set to measure a 60 mm compressed breast thickness. The top row of images was acquired for 1 min and formed from 60 000 counts. These images show the complete pattern with all tubes in the PEM field of view. The lower row of images was formed with only 14 000 counts. This series shows the coregistration tool and PEM detectors laterally displaced by 10 mm from the unit's axis of symmetry. The best-focused image is slice 5, which corresponds to the plane in which the tubes were placed.

Figure 8 shows the overlay of a PEM image after scaling to the corresponding mammogram film. (This image was taken from the upper row of Fig. 7, corresponding to the fifth image plane.) The mean distances between the PEM and x-ray images of each set of points are given in Table III. The sign of the distance indicates the position of the PEM image with respect to the mammogram. The average distance between the modalities ranges from 0.03 to 2.61 mm for each set of readings. The standard deviations in Table III reflect the ability to image and identify homologous points in each modality. These range from 0.01 to 0.91 mm (average: 0.24 mm) suggesting the measurement precision is better than the spatial resolution[12] of 2.1 mm. The X coordinate of the distances is greater than the instrument's spatial resolution. This is attributed to the difficulty in reading the scales on the rails on which the detectors travel, and a slight lateral play in these rails. (The scales have been made easier to read, and the play reduced since these experiments were performed.)

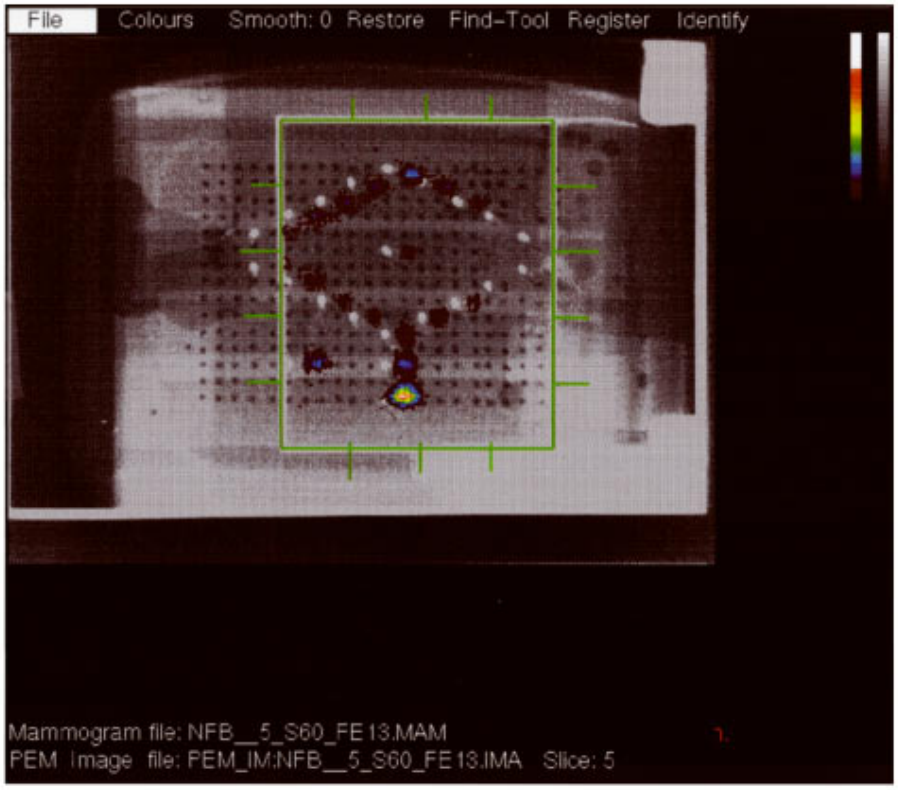

FIG. 8. Overlay of PEM image of the array of capillary tubes on a mammogram film illustrating the registration procedure. There is a lateral displacement of error of 2.25 mm between the PEM and x-ray images (Table III).

C. Patient study

A 48 year old woman presented with a radio-opaque mass in the superior lateral quadrant of the left breast in a routine mammogram. Two weeks later, she underwent a PEM study. The 5 min cranio-caudal (CC) PEM scan of the semicompressed left breast was performed 44 min after the injection of 75 MBq of FDG. Four days later, a modified radical mastectomy was performed on the left breast. Subsequent pathological examination of the tissue showed the presence of infiltrating intraductal carcinoma measuring $2.5\times2.2\times2.2$ cm classified as grade III on the Bloom and Richardson[25] scale. On this scale, a grade III tumor is poorly differentiated and metabolically more active than a grade I tumor.

The top row of Fig. 9 shows the seven CC images of the abnormal breast. These images were made with the energy discriminators set for 350–650 keV, and were made from 37 000 counts. The bottom row of Fig. 9 shows the images acquired for the ''assumed normal'' breast. Note the area of increased uptake (bright spot) in the suspicious breast. Figure 10 shows a zoomed image of the corresponding mammogram with the outline of the registration tool. The radio-opaque mass is visible as is a cluster of microcalcifications.

TABLE III. Mean distance (±std. dev.) between PEM and x-ray images of up to 18 points along both axes as a function of equivalent compression (60 and 70 mm) and lateral displacement (−30 to 30). The last column shows the number of points used.

Displacement in mm of PEM field-of-view with respect to mammogram center line	*X* distance (60 mm compress.)	*Y* distance (60 mm compress.)	*X* distance (70 mm compress.)	*Y* distance (70 mm compress.)	No. of visible points
−30	5.18±0.02	−0.70±0.06	2.56±0.06	−0.78±0.91	4
−20	5.15±0.13	−0.31±0.21	3.26±0.03	−1.33±0.42	11
−10	3.66±0.10	1.89±0.07	3.36±0.03	−1.90±0.48	17
0	−5.6 ±0.01	0.47±0.44	−1.70±0.20	−3.39±0.10	16
+10	1.87±0.13	0.84±0.21	2.69±0.08	−2.33±0.48	18
+20	2.25±0.14	−0.61±0.32	4.73±0.08	−2.87±0.10	10
+30	2.33±0.05	−1.40±0.07	3.38±0.47	−3.20±0.01	5
Average	2.12±0.08	0.03±0.19	2.61±0.14	−2.26±0.36	

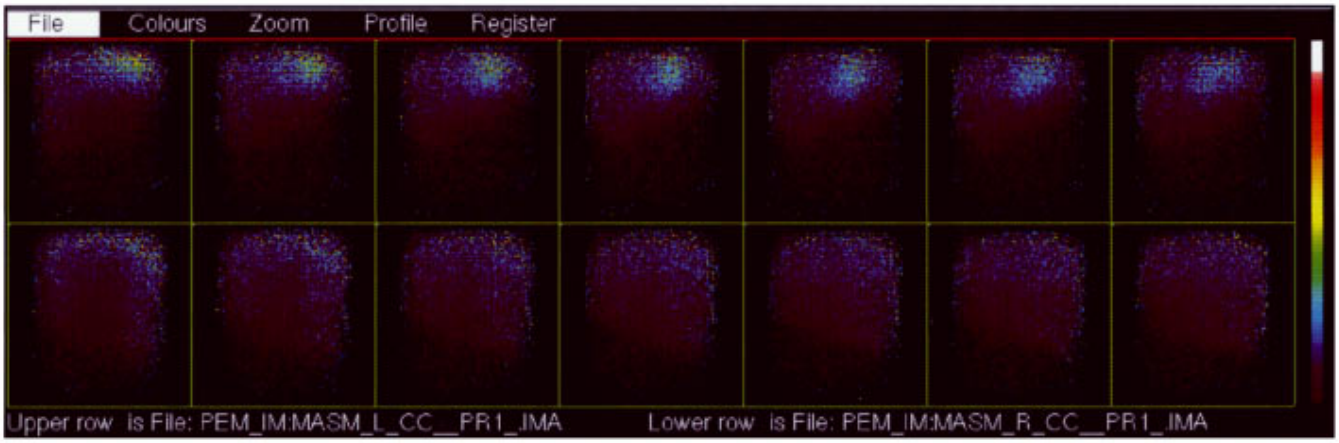

FIG. 9. Cranial-caudal view of abnormal left breast (top row) and right breast (bottom row). In the images, the breast appears pendant. The imaging time was 5 min, and the abnormality was clearly visible after 1 min.

Figure 11 shows the thresholded PEM image overlaid on the corresponding mammogram. The region of highest uptake corresponds well to the location of the microcalcifications on the mammogram.

VIII. DISCUSSION

In previous metabolic breast studies, registration with traditional modalities has been identified as a problem. Our instrument was designed from the beginning to allow integration of both structural and metabolic imaging. We have demonstrated that it can provide reproducible coregistered images.

The ability to view images almost in real time has considerable utility. In practice, our instrument can be used much like ultrasound in that the images appear almost instantly. The advantage of this is that other views can be added if an abnormality appears at the edge of the field, where the detectors are least efficient and the depth percep-

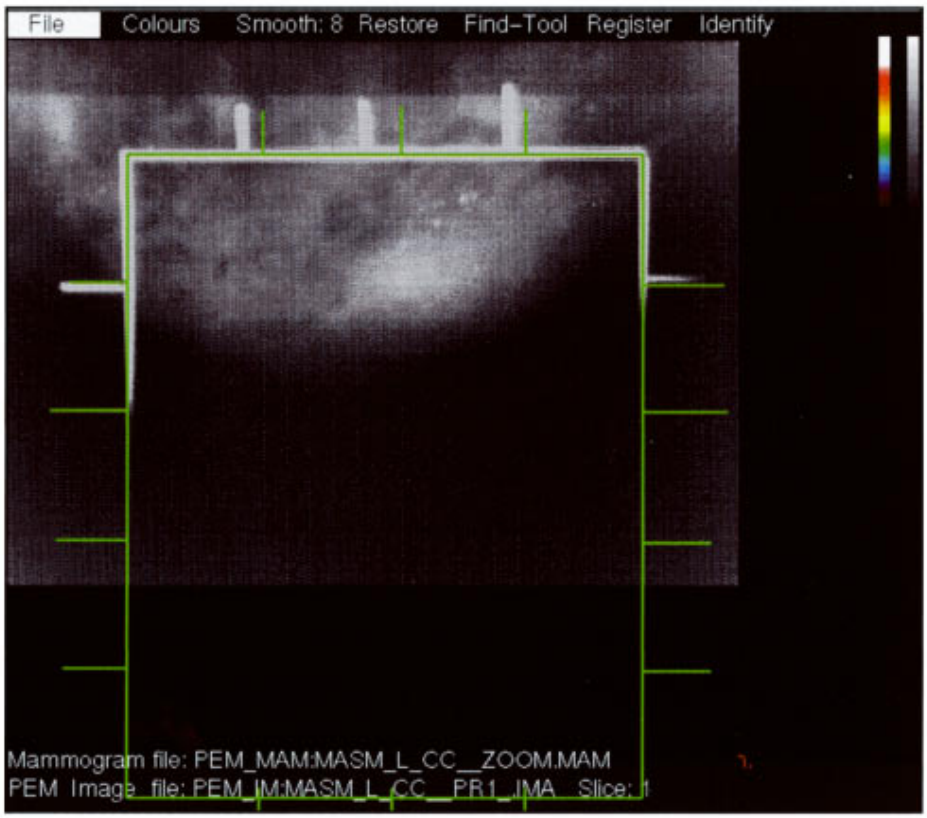

FIG. 10. Digitized mammogram shown with PEM registration display with outline of registration tool used to position PEM image. Note the microcalcifications near the top center of the registration tool.

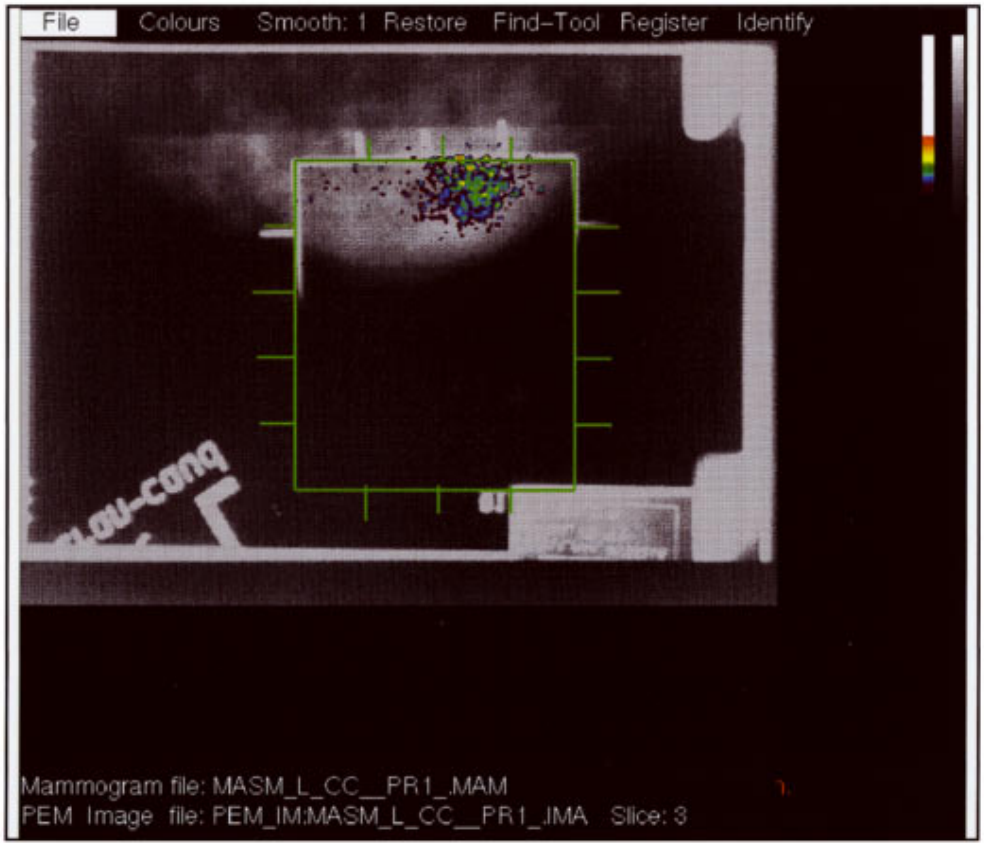

FIG. 11. PEM image showing increased metabolism in the same area as the mammographic abnormality.

tion is poor. Although the use of focal plane reconstruction, compared to other more sophisticated reconstruction algorithms, does not provide the most optimal image quality possible, the speed of this technique makes this instrument much more clinically feasible. We intend to develop an ''off-line'' limited angle reconstruction program algorithm which could provide more quantitative images of the cells' glucose metabolic rate.

At present, too few clinical studies have been done to draw any definitive conclusions on the potential future role of PEM in breast cancer detection. In our limited clinical experience we have found that the studies have been well tolerated by patients. The biggest problem has been to position the detectors over the suspicious region when it is close to the chest wall. Here we have found that MLO views allow deeper imaging.

IX. CONCLUSION

PEM's potential advantage over mammography is its ability to discern between malignant and benign tissues in three dimensions. The cost to modify a preexisting mammography accessory to accommodate this PEM instrument is much lower than purchasing a whole-body PET scanner. The injected dose required to obtain metabolic images with PEM is less than with whole-body PET (approximately 5 times less). After correcting for magnification factors, x-ray mammography images and PEM metabolic images can be accurately coregistered to obtain valuable information about the location and characterization of suspicious breast lesions.

ACKNOWLEDGMENTS

This research is funded by a generous grant from the National Cancer Institute of Canada's—Breast Cancer Research Initiative (Grant No. 6139). A.M.B. and J.L.R. both received scholarships from the ''Fonds pour la Formation de Chercheurs et l'Aide à la Recherche.''

The initial development of the detectors would not have been possible without the continuing support to one of us (C.J.T.) from the National Science and Engineering Council of Canada Grant No. OGP-0036672 and the Medical Research Council of Canada Grant No. SP30. We wish to acknowledge the MNI radiochemistry department which supplied the ^{18}F-FDG for these studies. We also thank the staff at the McGill University Physics Department machine shop, particularly Michel Champagne, for the construction of the detector housings and the PEM infrastructure. We would also like to thank Judith A. Haynie at Phillips Medical Systems for donating the magnification table used to build the PEM prototype. The patient studies were carried out with technical help of the staff of the Royal Victoria Hospitals Cedars Breast Clinic especially Doris Herusch and Bonnie Courte, and the Department of Nuclear Medicine, especially Lise Proulx.

[a]Electronic mail: alanah@rclvax.medcor.mcgill.ca
[b]Now at the British Columbia Cancer Agency, Vancouver, BC.

[1]L. H. Baker, ''Breast cancer detection demonstration project: 5 year summary report,'' Cancer **32**, 194–225 (1992).
[2]R. E. Bird, T. W. Wallace, and B. C. Yankaskas, ''Analysis of cancers missed at screening mammography,'' Radiology **184**, 613–617 (1992).
[3]O. Warburg, F. Wind, and E. Neglers ''On the metabolism of tumours in the body,'' in *Metabolism of Tumours*, edited by O. Warburg (Constable, London, 1930), pp. 254–270.
[4]R. S. Brown *et al.*, ''Intramural distribution of tritiated-FDG in breast carcinoma: Correlation with GLUT-1 expression and FDG uptake,'' J. Nucl. Med. **37**, 1024–1047 (1996).
[5]R. L. Wahl *et al.*, ''Primary and metastatic breast carcinoma: Initial clinical evaluation with PET with the radiolabeled glucose analogue 2-[F-18]-Fluoro-2-deoxy-Dglucose,'' Radiology **179**, 765–770 (1991).
[6]N. Y. Tse *et al.*, ''The application of PET imaging with fluorodeoxyglucose to the evaluation of breast disease,'' Ann. Surg. 27–34 (1992).
[7]O. E. Nieweg *et al.*, ''PET of glucose metabolism in breast cancer: Potential for tumor detection, staging, and evaluation of chemotherapy,'' Ann. (N.Y.) Acad. Sci. **68**, 423–435 (1993).
[8]O. E. Nieweg *et al.*, ''PET with fluorine-18-deoxyglucose in the detection and staging of breast cancer,'' Cancer **71**, 3920–3925 (1993).
[9]N. Avril *et al.*, ''Breast imaging with fluorine-18-FDG PET: Quantitative image analysis,'' J. Nucl. Med. **38**, 1187–1190 (1997).
[10]C. J. Thompson *et al.*, ''Positron emission mammography (PEM): A promising technique for detecting breast cancer,'' IEEE Trans. Nucl. Sci. **42**, 1012–1017 (1995).
[11]C. J. Thompson, K. Murthy, I. N. Weinberg, and F. Mako, ''Feasibility study for positron emission mammography,'' Med. Phys. **21**, 529–537 (1994).
[12]J. L. Robar, C. J. Thompson, K. Murthy, R. L. Clancy, and A. M. Bergman, ''Construction and calibration of detectors for high resolution metabolic breast imaging,'' Nucl. Instrum. Methods Phys. Res. A **392**, 402–406 (1997).
[13]I. Weinberg *et al.*, ''Preliminary results for positron emission mammography: Real-time functional breast imaging in a conventional mammography gantry,'' Eur. J Nucl. Med. **23**, 804–806 (1996).
[14]R. Freifelder and J. Karp, ''Dedicated PET scanners for breast imaging,'' Phys. Med. Biol. **42**, 2463–2480 (1997).
[15]W. Moses, T. Budinger, R. Huesman, and S. Derenzo, ''PET camera designs for imaging breast cancer and axillary node involvement,'' J. Nucl. Med. **36**, 69P (1995).
[16]G. Hutchins and A. Simon, ''Evaluation of prototype geometries for breast imaging with PET radiopharmaceutical,'' J. Nucl. Med. **36**, 69P (1995).
[17]A. Sandell, K. Erlandsson, and L. Bertenstam, ''A scanner for positron emission mammography,'' in *Metabolic Imaging of Cancer, Proceedings of the European Conference on Research and Application of Positron Emission Tomography in Oncology*, edited by A. Paans, J. Prium, E. Franssen, and W. Vaalburg (PET, Centrum AZG, 1996), pp. 88–89.
[18]S. F. Lay *et al.*, ''Breast biopsy-changing patterns during a five year period,'' Am. Surgeon **56**, 79–85 (1990).
[19]E. Kim, B. T. Kim, T. P. Hynie, D. A. Podoloff, W. H. Wong, D. J. Yang, R. S. Tilbury, G. Horobagyi, and S. Singletary, ''Evaluation of preoperative chemotherapy in patients with locoregionally advanced breast cancer using 18F-FDG PET,'' J. Nucl. Med. **33**, 828 (1992).
[20]D. M. Bruce *et al.*, ''Positron emission tomography: 2-deoxy-2-[18F]-fluoro-D-glucose uptake in locally advanced breast cancers,'' Eur. J. Surg. Oncol. **21**, 280–283 (1995).
[21]L. Chaiken *et al.*, ''Positron emission tomography with fluorodeoxyglucose to evaluate tumor response and control after radiation therapy,'' Int. J. Radiat. Oncol., Biol., Phys. **27**, 455–464 (1993).
[22]P. Bassa *et al.*, ''Evaluation of preoperative chemotherapy using PET with fluorine-18 fluoro-deoxyglucose in breast cancer,'' J. Nucl. Med. **37**, 931–938 (1996).
[23]R. L. Wahl, L. E. Quint, R. D. Cieslak, A. M. Aisen, R. A. Koeppe, and C. R. Meyer ''Anato-metabolic'' tumor imaging: Fusion of FDG PET with CT or MRI to localize foci of increased activity,'' J. Nucl. Med. **34**, 1190–1197 (1993).
[24]H. Loats, ''CT and SPECT image registration and fusion for spatial localization of metastatic processes using radiolabeled monoclonals,'' J. Nucl. Med. **34**, 562–566 (1993).
[25]H. J. G. Bloom and W. W. Richardson, ''Histological grading and prognosis in breast cancer. A study of 1409 cases which have been followed for 15 years,'' Br. J. Cancer **11**, 359–397 (1957).